Accepted Manuscript

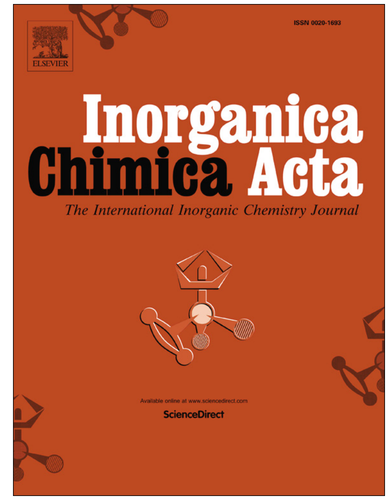

Increasing the histidine ‘density’ in tripodal peptides by gradual *N*-functionalization of *tris*(2-aminoethyl)amine (tren) with L-histidyl units: the effect on zinc(II) complexes

Ágnes Dancs, Katalin Selmeczi, István Bányai, Zsuzsanna Darula, Tamás Gajda

PII: S0020-1693(17)30678-3
DOI: http://dx.doi.org/10.1016/j.ica.2017.06.049
Reference: ICA 17698

To appear in: *Inorganica Chimica Acta*

Received Date: 29 April 2017
Revised Date: 10 June 2017
Accepted Date: 21 June 2017

Increasing the histidine 'density' in tripodal peptides by gradual *N*-functionalization of *tris*(2-aminoethyl)amine (tren) with L-histidyl units: the effect on zinc(II) complexes

Ágnes Dancs[a,b], Katalin Selmeczi[b], István Bányai[c], Zsuzsanna Darula[d] and Tamás Gajda[a*]

[a] *Department of Inorganic and Analytical Chemistry, University of Szeged, Dóm tér 7, H-6720 Szeged, Hungary*
[b] *Université de Lorraine – CNRS, UMR 7565 SRSMC, BP 70239, 54506 Vandœuvre-lès-Nancy, France*
[c] *Department of Colloid and Environmental Chemistry, University of Debrecen, Egyetem tér 1, H-4032 Debrecen, Hungary*
[d] *Institute of Biochemistry, Biologial Research Centre, Hungarian Academy of Sciences, Temesvári krt. 62, H-6724 Szeged, Hungary*

Dedicated to professor Imre Sóvágó, on the occasion of his 70th birthday

Abstract

Tripodal peptidomimetics have received increasing interest among others as efficient metal ion chelators. Most of these studies have focused on symmetrical, tri-substituted ligands. Our aim was to establish how the increasing donor group 'density', *i.e.* the gradual N-histidyl substitution, alters the coordination chemical properties of the tripodal platform. To this end we synthesized *mono*-, *bis*- and *tris*(L-histidyl)-functionalized tren derivatives (**L1**, **L2** and **L3**, respectively), and studied their zinc(II) complexes by pH potentiometry, ^{1}H NMR and MS spectroscopy. The three ligands provide a variety of donor sites, and consequently different stability and structure for their zinc(II) complexes depending on the pH and metal-to-ligand ratios. In the neutral pH range histamine-like coordination is operating in all cases. Due to the formation of macrochelate between the two/three $\{N_{im},NH_2\}$ binding sites, **L2** and **L3** have considerably higher zinc(II) binding ability than histamine, or any other simple peptide with N-terminal His unit. The situation is fundamentally different at higher pH. The tren-like subunit in **L1** acts as an anchoring site for amide deprotonation, and the $\{3NH_2,N^-,N_{tert}\}$ type coordination, a rare example where zinc(II)-amide N^- coordination takes place, results in outstanding stability. Although **L1** provides tight binding above pH 7, it forms only mononuclear species. However, the increasing level of functionalization in **L2** and **L3** allows the formation of oligonuclear complexes, and at threefold zinc(II) excess the three ligands share nearly the same amount of zinc(II). Moreover, the high histidine 'density' in **L2** and **L3** also provides the formation of imidazolato-bridged structures, which has never been observed before in zinc(II) complexes of simple linear peptides.

Introduction

Tripodal peptidomimetics have been receiving increasing interest in the last decades in order to create chiral receptor molecules [1,2], triple helical biomimetic materials [3], peptide-like dendrimers for *e.g.* drug delivery [4], organic catalysts [4] or metal ion chelators [5-12]. The metal ion binding properties of tripodal peptidomimetics can differ significantly from those of linear peptides. They have several beneficial attributes such as the pre-organized structure, a more favorable spatial distribution of the donor sites induced by the tripodal platform, and enhanced chelate effects due to the high 'density' of donor groups. By adequate substitution of the tripodal platform, it is relatively easy to fine-tune the (i) metal ion binding ability, (ii) the electronic structure and steric environment of the metal centers, and (iii) the nuclearity of the forming complexes. Indeed, by varying the substituents of the tripodal platforms, such ligands form both mono- [5-12] and oligonuclear [7,8,10-12] complexes, and provide tight binding for a range of metal ions, from Cu(I) [8], Cu(II) [9,12], Zn(II) [7,10,11] to Fe(III) [6]. Metal binding tripodal peptidomimetics can be strong metal ion sequestering agents [6-8] or may form efficient artificial metalloenzymes [9-12].

Due to the importance of histidine residues in metal ion binding of proteins, the coordination chemistry of histidine containing linear peptides is now well established [13,14]. Recently, we have synthesized two new non-protected histidine derivatives based on *tris*(2-aminoethyl)amine (tren) and nitrilotriacetic acid (nta) as tripodal platforms containing three N- (tren3his, **L3**) or C-terminal histidines (nta3his, Scheme 1), respectively [12]. The high donor group 'density' of the three histidines attached to the tripodal platforms provides the formation of highly stable mono- and oligonuclear copper(II) complexes. According to the different donor sets, these ligands behave differently in equimolar solutions. At neutral pH, $\{2N_{im},2NH_2\}$ and $\{N_{im},N^-,N_{tert},O\}$ types of coordination dominate with tren3his and nta3his, respectively, while at higher pH the participation of the tertiary amine in the fused chelate rings results in a unique $\{N_{im},N^-,N_{tert},N^-+N_{im}\}$ binding mode in both cases. The different number of unbound leg(s) at neutral pH results in different nuclearity of oligonuclear complexes [12].

The overwhelming majority of the studied metal binding tripodal peptidomimetics is symmetrical, tri-substituted derivatives. Our aim was to establish how the increasing donor group 'density', *i.e.* the gradual N-histidyl functionalization alters the coordination chemical properties of the tripodal platform. Since multihistidine environment around zinc(II) is very common in metalloproteins, we selected this metal ion to study the effect of increasing histidine density on complex formation. To this end we performed pH potentiometric, NMR and MS studies to determine the solution equilibrium and structural properties of the zinc(II) complexes formed in presence of *mono*-, *bis*- and *tris*(L-histidyl)-functionalized tren derivatives (**L1**, **L2** and **L3**, Scheme 1).

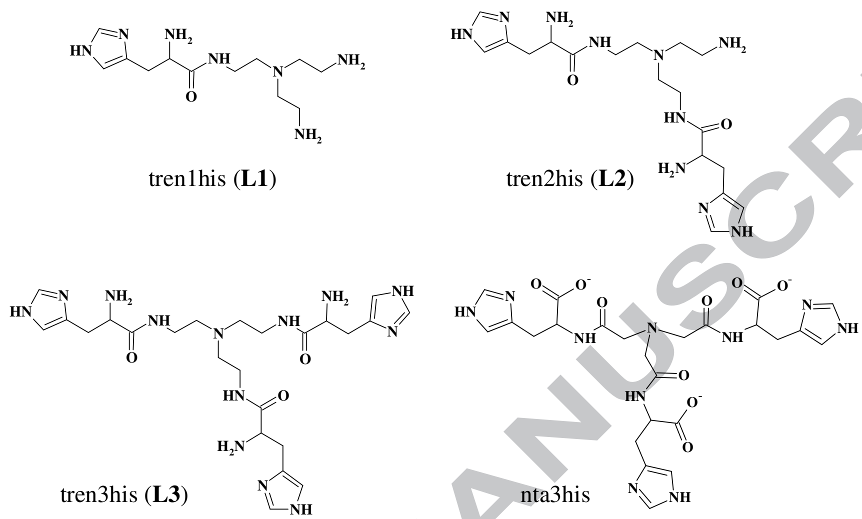

Scheme 1. Schematic structures of the studied ligands (**L1**-**L3**) and the close homolog nta3his [12].

2. Experimental section

2.1. Materials

Zinc(II) perchlorate (Sigma-Aldrich) stock solution was standardized complexometrically. pH-metric titrations were performed using 0.1 M NaOH standard solution (Sigma-Aldrich). L-histidine (Sigma-Aldrich), *tris*(2-aminoethyl)amine (tren, Sigma-Aldrich), *N,N'*-dicyclohexylcarbodiimide (DCC, Sigma), *N*-hydroxybenzotriazole (HOBt, Novabiochem), dichloromethane (Molar Chemicals), acetonitrile (VWR), trifluoroacetic acid (TFA, Sigma-Aldrich) and triisopropylsilane (TIS, Sigma-Aldrich) were analytically pure chemicals and used without further purification.

2.2. Preparation of the ligands

Starting materials Boc-His(Boc)-OH, monoBoc-tren and diBoc-tren were synthesized following literature procedures [15-17]. The synthesis of tren3his (**L3**) has already been reported in a previous work [12].

Synthesis of tren1his (L1). 0.42 g Boc-His(Boc)-OH (1.18 mmol) and 0.38 g diBoc-tren (1.09 mmol) were dissolved together in 50 ml dichloromethane, 0.25 g DCC (1.20 mmol) and 0.16 g HOBt (1.20 mmol) were added subsequently. The mixture was stirred overnight at rt. After filtration and evaporation of the solvent, the cleavage of Boc protecting groups was accomplished by a treatment of 95%-2.5%-2.5% TFA/TIS/water mixture. The cleaving mixture was evaporated using liquid nitrogen trap, the oily residue was dissolved in water, neutralized and purified by preparative HPLC (RP column: Supelco C18 5 μm, 25 cm × 10 mm geometry, eluent: 0 to 2% acetonitrile +0.1% TFA/15 min gradient elution mode, 3 ml/min flow rate, $t_R'_{\mathrm{tren1his}}$ = 3.7 min). After liophilization the trifluoroacetate salt of **L1** (70.6% yield) was obtained as white solid. ^{1}H NMR (500 MHz, D_2O/H_2O, pH 7.12) δ (ppm): 2.53 (t, 2H, J = 7.0 Hz, N_{tert}-CH_2^{funct}), 2.75 (t, 4H, J = 6.3 Hz, N_{tert}-CH_2^{free}), 2.94 (m, 2H, βCH_2), 3.03 (t, 4H, J = 6.3 Hz, CH_2-NH_2), 3.22 (m, 2H, CH_2-NHCO), 3.79 (t, 1H, J = 6.9 Hz, αC*H*), 6.95 (s, 1H, im-C^5*H*), 7.73 (s, 1H, im-C^2*H*). ^{13}C NMR δ (ppm): 30.8, 36.5, 37.1, 50.5, 51.3, 55.2, 117.1, 132.2, 136.2, 173.6. (ESI-MS *m/z* calcd for $C_{12}H_{26}N_7O$ $[M + H]^+$ 284.24, found 284.23 (z = 1). ESI MS, COSY, HMBC and HMQC spectra of **L1** are depicted in Figs. S1.1 and S2.1-3 (see Supplementary Informations).

Synthesis of tren2his (L2). 0.84 g Boc-His(Boc)-OH (2.36 mmol) and 0.27 g monoBoc-tren (1.10 mmol) were dissolved together in 50 ml dichloromethane, 0.47 g DCC (2.30 mmol) and

0.31 g HOBt (2.30 mmol) were added subsequently. The mixture was stirred overnight at rt. After filtration and evaporation of the solvent, the cleavage of Boc protecting groups was accomplished by a treatment of 95%-2.5%-2.5% TFA/TIS/water mixture. The cleaving mixture was evaporated using liquid nitrogen trap, the oily residue was dissolved in water, neutralized and purified by preparative HPLC (RP column: Supelco C18 5 μm, 25 cm × 10 mm geometry, eluent: 0 to 3.2% acetonitrile +0.1% TFA/20 min gradient elution mode, 3 ml/min flow rate, $t_R'_{tren2his}$ = 9.2 min). After liophilization the trifluoroacetate salt of **L2** (62.7% yield) was obtained as white solid. ^{1}H NMR (500 MHz, D_2O/H_2O, pH 6.70) δ (ppm): 2.47 (t, 4H, J = 6.9 Hz, N_{tert}-CH_2^{funct}), 2.69 (t, 2H, J = 6.2 Hz, N_{tert}-CH_2^{free}), 2.98 (m, 4H, βCH_2), 2.97 (m, 2H, CH_2-NH_2), 3.17 (m, 4H, CH_2-NHCO), 3.91 (t, 2H, J = 7.0 Hz, αCH), 6.97 (s, 2H, im-C^5H), 7.75 (s, 2H, im-C^2H). ^{13}C NMR δ (ppm): 29.9, 37.0, 37.1, 50.4, 52.0, 54.0, 117.0, 131.5, 136.1, 171.9. ESI-MS m/z calcd for $C_{18}H_{33}N_{10}O_2$ $[M + H]^+$ 421.26, found 421.32 (z = 1). ESI MS, COSY, HMBC and HMQC spectra of **L2** are depicted in Figs. S1.2 and S2.4-6 (see Supplementary Informations).

2.3. Potentiometry

The protonation and coordination equilibria were investigated by pH-potentiometric titrations in aqueous solutions (I = 0.1 M NaCl and T = 298.0 ± 0.1 K) under argon atmosphere. The titrations were performed using a PC controlled Dosimat 665 (Metrohm) automatic burette and an Orion 710A precision digital pH-meter. The Metrohm micro glass electrode (125 mm) was calibrated by the titration of hydrochloric acid and the data were fitted using the modified Nernst-equation [18]:

$$E = E_0 + K \cdot \log[\mathrm{H}^+] + J_{\mathrm{H}} \cdot [\mathrm{H}^+] + \frac{J_{\mathrm{OH}} \cdot K_{\mathrm{w}}}{[\mathrm{H}^+]}$$

where J_H and J_{OH} are the fitting parameters representing the acidic and alkaline error of the glass electrode, respectively ($K_w = 10^{-13.75}$ is the autoprotolysis constant of water [19]). The parameters were calculated by the non-linear least squares method. The formation of the complexes was characterized by the general equilibrium process:

$$\mathrm{pM + qH + rL} \xrightleftharpoons{\beta_{\mathrm{M_pH_qL_r}}} \mathrm{M_pH_qL_r}$$

$$\beta_{\mathrm{M_pH_qL_r}} = \frac{[\mathrm{M_pH_qL_r}]}{[\mathrm{M}]^p[\mathrm{H}]^q[\mathrm{L}]^r}$$

where M denotes the metal ion and L the fully deprotonated ligand molecule. Charges are omitted for simplicity, but can be easily calculated taking into account that the fully deprotonated ligands (at pH 11) are neutral. The protonation constants of the ligands and the formation constants of the complexes were calculated by the PSEQUAD computer program [20] from 4, and 5-7 independent titrations, respectively (*ca*. 90 data points per titration). The metal ion concentrations varied between 0.6-2.6×10^{-3} M applying 2:1, 1.5:1, 1:1 and 1:2 metal-to-ligand ratios.

2.4. ^{1}H NMR spectroscopy

^{1}H NMR titrations were performed on a Bruker Avance DRX400 or Bruker Avance DRX500 spectrometer at 298 K in aqueous solutions, using a capillary filled with D_2O (for **L1** and **L2**) or with H_2O/D_2O 90/10% mixed solvent (**L3**). The chemical shifts (δ) were measured with respect to dioxane as internal reference and converted relative to $SiMe_4$, using $\delta_{dioxane}$ = 3.70 (^{1}H) and 66.5 (^{13}C). The initial ligand concentrations were 1.7×10^{-3} M, 1.8×10^{-3} M and 1.8×10^{-3} M for **L1**, **L2** and **L3** ligand systems, respectively. Ionic strength of 0.1 M NaCl was applied. The pH was adjusted to the desired values using NaOH solution. 1D ^{1}H NMR spectra were recorded by using presat or watergate sequences in order to reduce water signal. The assignment of the proton and carbon signals of the ligands was based on COSY, HMQC and HMBC 2D spectra (see Electronic Supplementary Information, Section 2). DOSY measurements were performed with solvent suppression at 293 K. Three sets of spectra were recorded, following the preparation of the complex solution and repeated after 90 and 156 h, in order to verify the kinetic stability and reproducibility of the system during the experiment. A stimulated spin echo pulse sequence was employed using bipolar gradient pulses to decrease eddy currents (BIPLED) at 293 + 0.2 K. A Eurotherm unit was used for stabilizing or regulating the temperature with air flow through a Bruker BSCU 05 cooling unit. The diffusion coefficient of water (D_2O) was determined in every sample in order to check the state of the instrument. Typical parameters for diffusion experiments were diffusion times of = 15 - 40 ms and lengths of gradient pulses of = 4 ms . The diffusion data were evaluated according to the equation:

$I = I_0 \exp(-D_{obs}(\; - \; /3) \; ^2 \; ^2 G^2)$

The pulsed gradient strength (G) increased with 64 square distant steps from 0 to approximately 50 G cm–1. $D_{obs}\gamma^2$ was calculated after fitting the exponential curve on the measured echo intensity, I, as a function of G^2 (determined by the number of experiments). The real diffusion coefficient D was calculated as $\kappa D_{obs}\gamma^2$, where κ is the calibration constant of the gradient. The calibration of the gradient was made for D_2O, using the known D =1.62 10^{-9} m^2s^{-1} [21] (extrapolated to 293K from the T function). Bruker TopSpin 2.0 software was used for post processing. Im-C^2-deuterated samples of **L2** were prepared as following: the ligand was dissolved in D_2O, 20 eq. NaOD was added, then the solution was incubated at 50°C. After 24 h the pH was adjusted by DCl and 2 eq. zinc(II) solution was added.

2.5. Mass spectrometry

Molecular weight analyses of the ligands and their zinc(II) complexes were carried out by Electrospray Ionization (ESI) and Matrix-Assisted Laser Desorption/Ionization (MALDI) mass spectrometric measurements. Spectra were recorded on a Bruker MicroTOFQ ESI and a Bruker Reflex III MALDI-TOF mass spectrometers. All spectra were obtained in positive mode. Acquisition parameters for ESI-MS measurements were the following: capillary voltage of 4.5 kV, 4.0 l/min dry gas flow, collision cell RF 250.0 Vpp. Samples were prepared as aqueous solutions, pH was adjusted, then they were diluted in acetonitrile/water 50%-50% mixture.

Sample preparation for MALDI-TOF MS measurements were the following: 1 µl of the samples was spotted onto the MALDI target plate and let dry before adding 0.5 µl of the matrix solution (2,6-dihydroxyacetophenone (DHAP) in acetonitrile-water 50/50%). Mass spectra were recorded in the positive reflectron mode collecting 200 shots for each sample (m/z range: 250-2000). External calibration affording ±200 ppm mass accuracy was performed using peptide standards. DHAP matrix was obtained from Sigma-Aldrich.

3. Results and discussion

3.1. Protonation equilibria of the ligands

The protonation constants and p*K* values of **L1**-**L3** derived from pH-potentiometric titrations are collected in Table 1. The identification of the deprotonating groups has been supported by pH-dependent ^{1}H NMR measurements (Electronic Supplementary Information, Figs. S3.1, S3.2 and S3.5). The p*K* values of tren-NH_2 and αCH-NH_2 amino nitrogens are between p*K* = 9.04-9.90 and 6.34-7.85, respectively. The increasing overall charge of the ligands at acidic pH results in increased acidity of imidazolium rings (p*K* = 3.87-5.41).

Table 1. Protonation constants and p*K* values of the studied ligands (I = 0.1 M NaCl, T = 298 K, estimated error of last digits in parentheses).

	tren1his (**L1**)		tren2his (**L2**)		tren3his (**L3**) [12]	
	logβ	p*K*	logβ	p*K*	logβ	p*K*
H_6**L**			36.46(1)	2.33	35.29(1)	3.87
H_5**L**			34.13(1)	4.62	31.42(1)	4.82
H_4**L**	31.04(1)	5.03	29.51(1)	5.41	26.60(1)	5.20
H_3**L**	26.01(1)	7.07	24.10(1)	6.82	21.40(1)	6.34
H_2**L**	18.94(1)	9.04	17.28(1)	7.69	15.06(1)	7.21
H**L**	9.90(1)	9.90	9.59(1)	9.59	7.85(1)	7.85

The p*K* of the tertiary amino group could be determined only for **L2**, which was also supported by the pH dependence of ^{1}H NMR spectra (Fig. S3.2). The ^{1}H NMR spectra of **L3** also show considerable shifts between pH 1.8-6.0 for the signals of both imidazole and tren-CH_2 protons (Fig. S3.5), although the p*K* of the tertiary amino group cannot be determined from the potentiometric data. These observations suggest an extensive H-bonding network involving the imidazolium/imidazole rings and the neutral tertiary nitrogen in **L3**. Such shift of ^{1}H NMR signals below pH 4 was not observed in case of **L1** (Fig. S3.1), which suggests low basicity of tertiary nitrogen in **L1**, similarly to tren itself [22].

*3.2. Zinc(II) complexes of tren1his (**L1**)*

Four differently protonated mononuclear species could be identified by potentiometry in the Zn(II)-**L1** system (Table 1, Fig. 1). At the beginning of complex formation (pH 4.5-5.5) all ^{1}H NMR signals of histidine unit are significantly broadened (Fig. 2A,B). Even though ZnH_2**L1** complex is not produced in higher quantities than 40%, the selective broadening on the ^{1}H NMR spectra indicates that the histidine unit is bound to zinc(II) in this species in a

Table 2. Formation and deprotonation constants of zinc(II) complexes of **L1**, **L2** and **L3** (I = 0.1 M NaCl, T = 298 K, estimated error of last digits in parentheses).

	tren1his (**L1**)		tren2his (**L2**)		tren3his (**L3**)	
	logβ	pK	logβ	pK	logβ	pK
ZnH_3L					24.76(2)	4.90
ZnH_2L	23.45(3)	6.45	22.37(1)	6.07	19.86(1)	5.42
ZnHL	17.00(3)		16.30(1)	8.10	14.44(1)	6.49
ZnL			8.20(3)	8.72	7.95(1)	8.10
$ZnH_{-1}L$	4.16(2)	10.73	-0.52(3)	9.92	-0.15(2)	10.24
$ZnH_{-2}L$	-6.57(4)		-10.44(3)		-10.39(2)	
$Zn_2H_{-2}L$			-2.81(2)	8.53		
$Zn_2H_{-3}L$			-11.34(2)	10.78		
$Zn_2H_{-4}L$			-22.12(4)			
Zn_3L_2					22.87(4)	
$Zn_3H_{-2}L_2$					9.62(3)	8.04
$Zn_3H_{-3}L_2$					1.58(4)	
$Zn_3H_{-4}L_2$					-7.32(4)	8.90

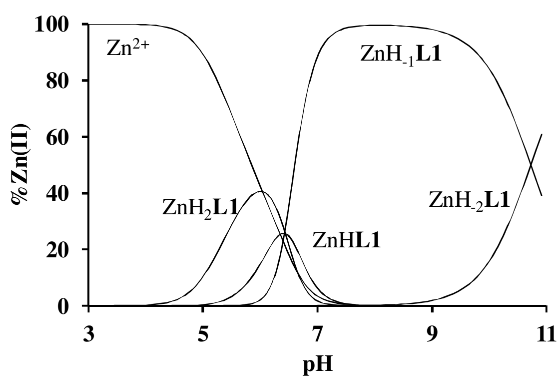

Fig. 1. Speciation diagrams in Zn(II)-**L1** 1:1 system ($c_{\mathbf{L1}} = c_{Zn(II)}$ = 0.001 M, I = 0.1 M NaCl, T = 298 K).

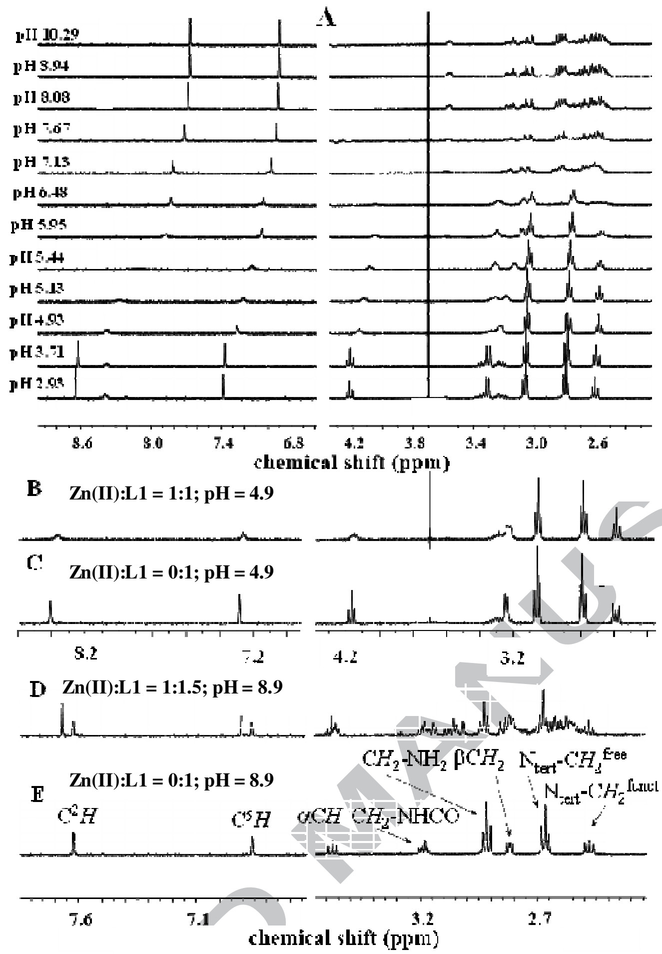

Fig. 2. pH-dependent ^{1}H NMR spectra of Zn(II)-**L1** 1:1 system (A,B), 1:1.5 system (D) and comparison with the spectra of free ligand (C,E). In H_2O, dioxane reference (3.70 ppm), $c_{\mathbf{L1}}$ = 0.0016 M, I = 0.1 M NaCl, T = 298 K.

histamine-like binding mode {N_{im},NH_2} (Scheme 2). The log$K$ value for the process Zn^{2+} + H_2**L1** = ZnH_2**L1** (log$K$ = log$\beta_{ZnH_2\mathbf{L1}}$ - log$\beta_{H_2\mathbf{L1}}$ = 4.51) also supports this type of coordination [23].

The formation of ZnH_{-1}**L1**, a dominant complex between pH 7.0-10.0, occurs through three strongly overlapped deprotonations (ZnH_2**L1** = ZnH_{-1}**L1** + $3H^+$), which are so cooperative that Zn**L1** could not be detected at all. In parallel (pH 6.0-7.5), remarkable changes can be observed on the NMR spectra. All CH_2 signals first broaden then sharpen to result a complex spectrum in the basic pH range (Figs. 2A,D). The source of this complicated peak set is the slow ligand exchange rate of ZnH_{-1}**L1**, and the inequivalence of all CH_2 protons related to the metal-bound ligand. 2D COSY spectrum of this region supports that both tren-CH_2 and βCH_2 groups possess strongly inequivalent hydrogens being coupled with the neighboring protons (Fig. S5.1).

The slow ligand exchange observed for ZnH_{-1}**L1** indicates that the 'extra' deprotonation is related to the formation of amide-bound species (and not to mixed hydroxo complexes) [24], which is also supported by its ESI-MS spectrum (Fig. S6.1). Besides, the complete formation of ZnH_{-1}**L1** at pH 7 suggests zinc(II) protomoted deprotonation and coordination of all three primary amino groups (their p*K*s in the free ligand are 7.07, 9.04, 9.90). Although the tertiary amino group is deprotonated at pH 7 even in the absence of zinc(II), the preferred formation of fused chelate rings and the inequivalence of all tren-CH_2 protons support its coordination. The simultaneous coordination of amide-, NH_2- and imidazole nitrogens is unlikely in the case of N-terminal His fragments [13,14], therefore our observations indicate $\{3NH_2,N^-,N_{tert}\}$ type binding in ZnH_{-1}**L1** (Scheme 2), which is in accordance with the well-known preference of tren derivatives for the trigonal bipyramidal geometry [22]. The NMR spectrum of ZnH_{-1}**L1** at ligand excess (Fig. 2D) shows only a slight upfield shift for the αCH signal, which is the result of two opposing effects, the coordination of the α-amino group and the deprotonation of the nearby amide nitrogen. In consequence of the saturated coordination sphere in ZnH_{-1}**L1**, the p*K* of the subsequent deprotonation is rather high (10.73), since the coordinating hydroxide ion should displace one of the bound nitrogens.

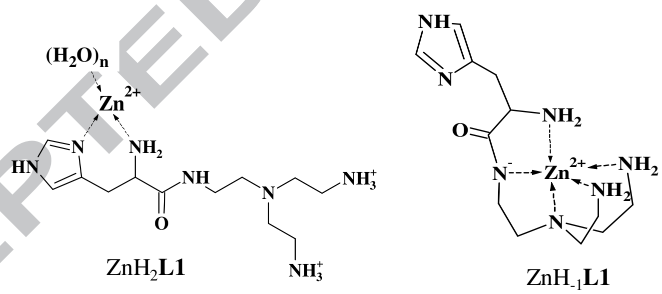

Scheme 2. Proposed structure of the main Zn(II)-**L1** complexes.

*3.3. Zinc(II) complexes of tren2his (**L2**)*

In presence of **L2**, water soluble complexes are formed even at 2:1 zinc(II)-to-ligand ratio, indicating the formation of both mono- and dinuclear complexes. The formation constants of the complexes are listed in Table 1, their speciation is depicted in Fig. 3. In the equimolar system, monozinc(II) complexes dominate in the whole studied pH range. The complexation starts with the formation of ZnH_2**L2** around pH 4.5. The ^1H NMR spectra around pH 5 show notable broadening for the imidazole proton signals (Fig. S3.3), indicating their role in the metal binding. Since both imidazole rings and one of the α-amino groups are deprotonated by metal ion assistance in ZnH_2**L2**, and the log$K$ for the process Zn^{2+} + H_2**L2** = ZnH_2**L2** (log$K$ = log$\beta_{ZnH_2\mathbf{L2}}$ - log$\beta_{H_2\mathbf{L2}}$ = 5.09) is higher than for **L1**, a histamine-type binding with the additional coordination of the second imidazole ring $\{2N_{im},NH_2\}$ can be assumed in this species. The deprotonation of ZnH_2**L2** (pK = 6.07) results in the formation of ZnH**L2**, a dominant complex between pH 6.0-8.0. The zinc(II)-assisted deprotonation of the remaining $\alpha CH\text{-}NH_3^+$ results in the formation of *bis*-histamine-type $\{2N_{im},2NH_2\}$ coordination, which

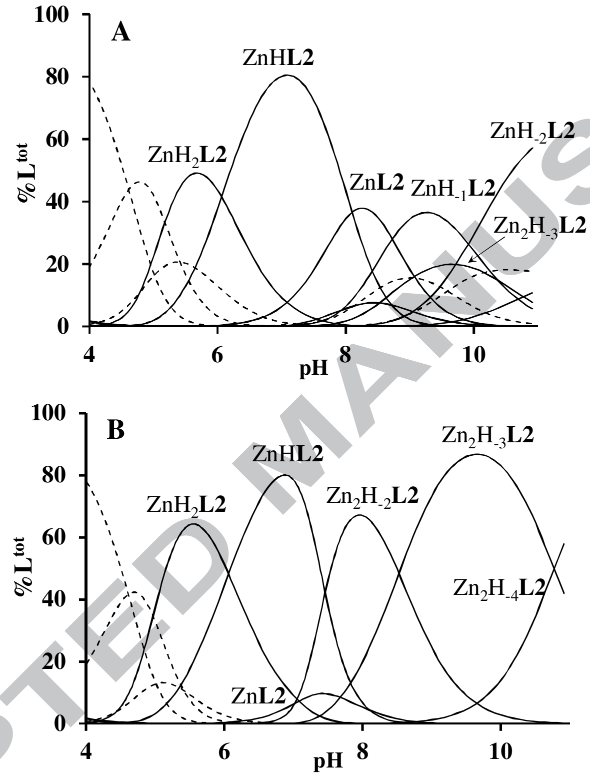

Fig. 3. Speciation diagrams in Zn(II)-**L2** 1:1 (A) and 2:1 (B) systems ($c_{\mathbf{L2}}$ = 0.001 M, $c_{Zn(II)}$ = 0.001 and 0.002 M, I = 0.1 M NaCl, T = 298 K), dashed lines represent unbound ligand (H_x**L2**) species.

involves a macrochelate between the two His units (Scheme 3). The formation of this macrochelate is favorable, since the basicity corrected stability constant of ZnH**L2** (log$K$ = log$\beta_{ZnH\mathbf{L2}}$ - log$\beta_{H_5\mathbf{L2}}$ = -17.13) is more than 4 units higher than that of the analogous Zn(histamine)$_2$ complex (log$K$ = logβ_{ZnL_2} - 2logβ_{H_2L} = -21.71 [23]). Interestingly, the presence of this macrochelate induces inequivalence of the CH_2 protons of the functionalized arms, which can be clearly seen on the $N_{tert}\text{-}CH_2^{funct}$ signals at ~ 2.4 ppm (Fig. 4B). The considerable downfield shift of αCH protons, close to the coordinated NH_2, as compared to the free ligand, is also noteworthy.

Above neutral pH, three overlapping deprotonation steps take place to result Zn**L2**,

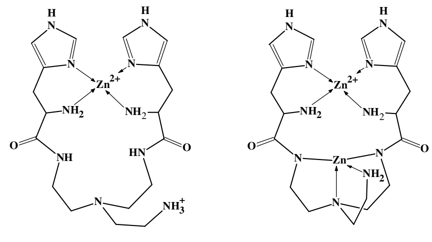

Scheme 3. Proposed structures of main Zn(II)-**L2** complexes.

ZnH_{-1}**L2** and ZnH_{-2}**L2**, beside a small amount of dinuclear complexes. During these processes the inequivalence of N_{tert}-CH_2^{funct} protons ceased, and the signals of αCH protons are strongly upfield shifted (~3.5 ppm, Fig. 4E) indicating rearrangement in the coordination sphere. However, the general broadening of the ^{1}H NMR signals (Figs. 4.D,E and S3.3) allows to draw only limited conclusions. Nevertheless, the broad spectra indicate that the 'extra' deprotonations related to the formation of mixed hydroxo species (Zn**L2**$(OH)_x$, x = 1,2), since the deprotonation of the amide nitrogen(s) would result in slow ligand exchange (*i.e.* sharp signals, like in the Zn(II)-**L1** or Zn(II)-Gly/AlaHis systems [24]).

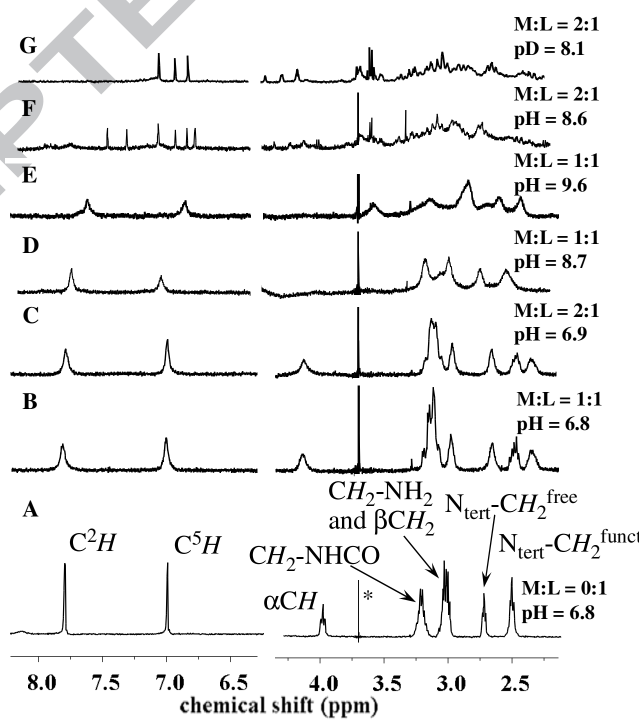

Fig. 4. [1]H NMR spectra of **L2** (A), Zn(II)-**L2** 1:1 (B,D,E) and Zn(II)-**L2** 2:1 (C,F, and G after deuteration of im-C[2] group) systems ($c_{\mathbf{L2}}$ = 0.0018 M, I = 0.1 M NaCl, T = 298 K). Marked* signal corresponds to dioxane reference at 3.70 ppm.

At metal excess, the evaluation of potentiometric data indicated the formation of three dinuclear complexes (Fig. 3B) with compositions of Zn_2H_{-2}**L2**, Zn_2H_{-3}**L2** and Zn_2H_{-4}**L2**. Their formation starts around pH 7 (Fig. 3B), which is in good agreement with the ^{1}H NMR spectra recorded at twofold metal excess, since up to pH 7 the spectral features are identical to that observed at Zn(II)-**L2** 1:1 ratio (Figs. 4B,C). Above neutral pH, several αCH proton signals can be seen, and more importantly six sharp signals appeared in the aromatic region of ^{1}H NMR spectrum (Figs. 4.F, 5.A and S3.4). The latter indicates three chemically different environments for the imidazole rings with nearly equal populations in the slow exchanging oligonuclear complexes. 2D TOCSY measurements (Fig. S5.2) and ^{1}H NMR spectrum of the complex(es) deuterated at the imidazole C^2 carbon (Fig. 4G) allowed the identification of the C^2H/C^5H pairs. Accordingly, at pH 8.2 the C^2H signals are strongly upfield-shifted by 0.29, 0.46 and 1.05 ppm in the slow exchanging oligonuclear complexes, as compared to the free ligand (Fig. 5B).

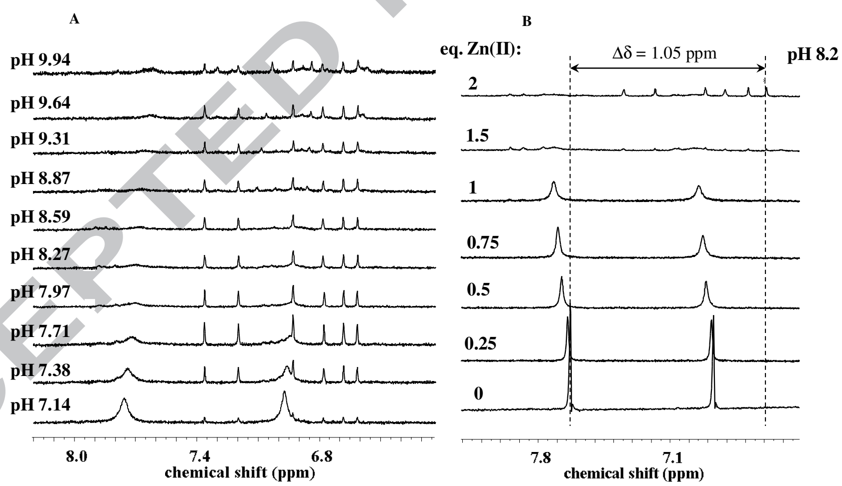

Fig. 5. Aromatic region of ^{1}H NMR spectra of Zn(II)-**L2** system. (A): pH dependence at Zn(II)-**L2** 1.9:1 ratio; (B): dependence on the Zn(II)-**L2** ratios at pH 8.2 (in H_2O, $c_{\mathbf{L2}}$ = 0.0018 M, I = 0.1 M NaCl, T = 298 K).

The 'extra' deprotonation observed for the oligonuclear species between pH 7-8 could be assigned to (i) deprotonation of coordinated water molecule(s), (ii) metal-promoted deprotonation of amide nitrogen(s) or (iii) formation of μ-imidazolato-bridge between two zinc(II) ions. Among these processes only (ii) and (iii) may lead to slow ligand exchange processes and notable shift of imidazole proton signals. It is worth to mention that the strongly related *N,N'*-di-L-histidylethane-1,2-diamine (dhen) ligand also forms imidazolato-bridged oligozinc(II) complexes in the same pH range [23]. The increased electron density on the imidazolate ring obviously results in remarkable upfield shift of C^2H signals (up to ~2.2 ppm [23,25,26]), as compared to the free ligand. On the other hand, in the Zn(II)-GlyHis system [24] the coordination of imidazole ring and the deprotonation of nearby amide nitrogen also resulted in 0.2-0.4 ppm upfield shift of the imidazole and αCH signals. In the present system, the wide range of chemical shifts of imidazole and αCH signals upon metal ion binding (Figs. 4.F, 5) indicates the presence of both amide- and imidazolate-bound zinc(II) centers.

The *bis*-histamine-type coordination of zinc(II) in ZnH**L2** provides a preorganized tren-like $\{NH_2,N_{tert},2N^-\}$ binding site for the second metal ion (Scheme 3), *i.e.* the deprotonation of the amide nitrogens is promoted by the anchoring $\{NH_2^{tren},N_{tert}\}$ chelate. This binding mode explains the direct transformation of ZnH**L2** into Zn_2H_{-2}**L2** (Fig. 3B), and also the fact that dinuclear complexes are formed only at metal ion excess (Fig. 5B), in parallel with the zinc(II)-promoted deprotonation of NH_3^+ of the free tren arm. However, the two imidazole moieties in Zn_2H_{-2}**L2** cannot exist in three chemically different environments with nearly equal populations; therefore, more than one species must be present under these conditions.

In order to explain the above-mentioned observations, we assume a dimerization process of $2Zn_2H_{-2}$**L2** = $(Zn_2H_{-2}$**L2**$)_2$, through the formation of two imidazolato-bridges and the re-protonation of two zinc(II)-bound amide nitrogens (see Fig. S4.1 and a more detailed discussion in ESI Section 4). The simultaneous presence of the two complexes (Zn_2H_{-2}**L2** and $(Zn_2H_{-2}$**L2**$)_2$) is probably the simplest way to explain the six sharp signals observed in the aromatic region of the NMR spectra at 2:1 Zn(II)-**L2** ratio (Fig. 5).

The characteristic spectral patterns of the oligonuclear complexes are present in the NMR spectra over a wide pH range (pH 7-10, Fig. 5.A), meaning that the basic skeletons of these species are unchanged during the next observed deprotonation (Zn_2H_{-2}**L2** = Zn_2H_{-3}**L2** + H^+), suggesting the formation of mixed hydroxo complexes. On the other hand, new sharp peaks appear in the imidazole region around pH 10 (Fig. 5A), which indicates structural reorganization within the oligonuclear complexes. However, this deprotonation step (Zn_2H_{-3}**L2** = Zn_2H_{-4}**L2** + H^+, pK = 10.78) is complete only above pH 11, therefore detailed ^1H NMR investigations were not performed.

Consequently, the fitting of potentiometric data by only dinuclear complexes is an oversimplified model of the real situation. Nevertheless, it can describe the titration curves correctly, since the equilibrium constants of reaction $ZnH\mathbf{L2} + Zn^{2+} = (1/n)(Zn_2H_{-x}\mathbf{L2})_n + (x+1)H^+$ for different values of *n* and different kind of deprotonation processes are nearly identical.

*3.4. Zinc(II) complexes of tren3his (**L3**)*

Potentiometric titrations, MALDI-TOF MS and ^{1}H NMR measurements were carried out in order to gain information on the Zn(II)-**L3** complexes. Clear solution was obtained in the whole studied pH range at 1:1 and 1.5:1 metal-to-ligand ratio, but precipitation was observed above pH 7 at twofold metal ion excess. Accordingly, the evaluation of potentiometric data indicated the formation of complexes with $ZnH_x\mathbf{L3}$ and $Zn_3H_x\mathbf{L3}_2$ stoichiometries, similarly to the previously reported Cu(II)-tren3his system [12]. The presence of these species has been verified by MALDI-TOF MS measurements. The detected *m/z* values and isotopic distribution patterns are in good agreement with the calculated spectra for $[ZnH_{-1}\mathbf{L3}]^+$ (= $[C_{24}H_{38}N_{13}O_3Zn]^+$) and $[Zn_3H_{-4}\mathbf{L3}_2(ClO_4)]^+$ (= $[C_{48}H_{74}N_{26}O_{10}ClZn_3]^+$) (Fig. 6).

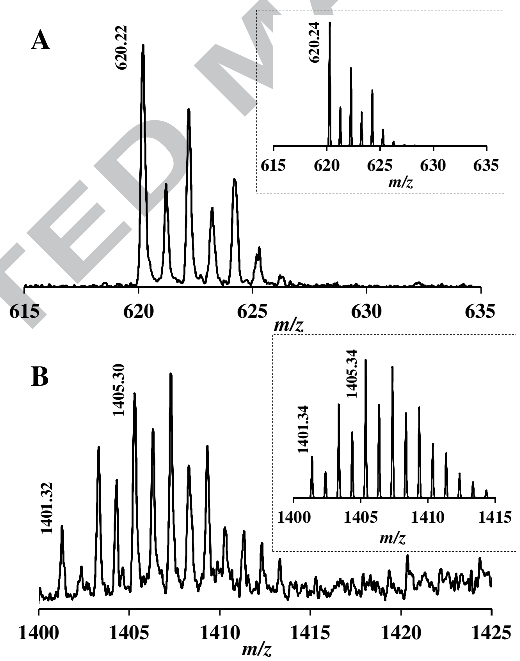

Fig. 6. MALDI-TOF MS spectra measured in the Zn(II)-**L3** 1:1 (A) and 3:2 (B) systems. Insert: calculated spectra of the corresponding complex ($[C_{24}H_{38}N_{13}O_3Zn]^+$ and $[C_{48}H_{74}N_{26}O_{10}ClZn_3]^+$, respectively).

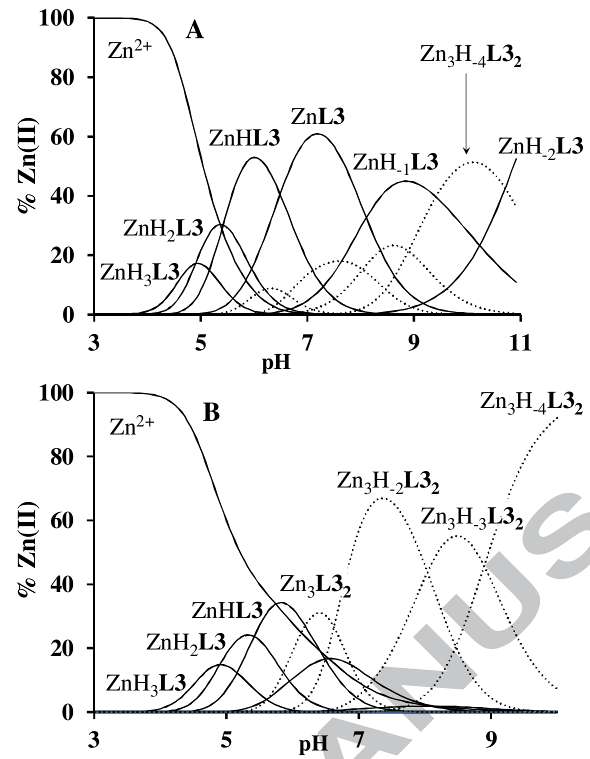

Fig. 7. Speciation diagrams in Zn(II)-**L3** 1:1 (A) and 1.5:1 (B) systems ($c_{\mathbf{L3}}$ = 0.001 M, $c_{Zn(II)}$ = 0.001 and 0.0015 M, I = 0.1 M NaCl, T = 298 K), dotted lines represent trinuclear (Zn_3H_{-x}**$L3_2$**) species.

The formation constants of the complexes are listed in Table 2, their speciation is depicted in Fig. 7. Between pH 4-7, three overlapped deprotonations take place in equimolar solution, leading to the major species ZnH**L3** (at pH ~ 5.8) and Zn**L3** (at pH ~ 7.2). The ^{1}H NMR spectra in this pH range (Figs. 8A,B and S3.6) show similar behavior to that of the Zn(II)-**L2** system (Fig. 4), *i.e.* downfield shift upon coordination of both imidazole and αCH signals, and inequivalence of N_{tert}-CH_2 protons at ~ 2.4 ppm, suggesting the formation of the similar macrochelate with *bis*-histamine-like binding. However, several facts indicate the additional coordination of the third histidine 'pod', too. First, the pK values of the protonated complexes (p$K_{ZnH_2\mathbf{L3}}$ = 5.42, p$K_{ZnH\mathbf{L3}}$ = 6.49) are lower than those of the free ligand (p$K_{H_2\mathbf{L3}}$ = 7.21, p$K_{H\mathbf{L3}}$ = 7.85), and also than the analogous copper(II) containing species (p$K_{CuH_2\mathbf{L}}$ = 5.55, p$K_{CuH\mathbf{L}}$ = 6.92 [12]). Second, the predominance diagram of the Zn(II)-**L2**-**L3** 1:1:1 ternary system indicates considerably stronger metal binding ability for **L3** around pH 6-7 (Fig. S7.1). As a consequence, either 5N or 6N coordination can be proposed for Zn**L3** (Scheme 4).

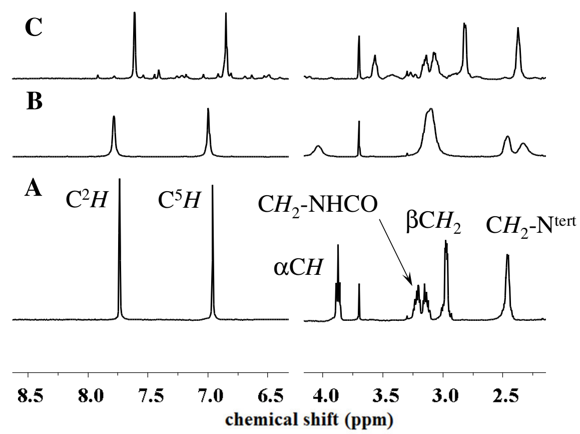

Fig. 8. ^{1}H NMR spectra of **L3** (A) and Zn(II)-**L3** 1:1 (B,C) systems. pH = 7.2 (A), 7.3 (B) and 9.8 (C). (in H_2O/D_2O, dioxane reference (3.70 ppm), $c_{\mathbf{L3}} = 0.0023$ M, $I = 0.1$ M NaCl, T = 298 K).

Under basic conditions the complex Zn**L3** releases two additional protons (pK = 8.10 and 10.24). The ^{1}H NMR spectra recorded in equimolar solution above pH 7 (Fig. S3.6) are again similar to those of the Zn(II)-**L2** system (Fig. S3.3), the inequivalence of N_{tert}-CH_2 protons ceased, and the signals of αCH-protons are strongly upfield shifted. The formation of slow exchanging complexes was not detected. The coordination of amide nitrogen(s) is indeed unlikely, since N-terminal histidines with {N_{im},NH_2} binding site do not act as anchor for amide deprotonations, and such processes have never been observed in Zn(II)-His-Gly and related systems [13,27-29]. These deprotonations are more likely related to the formation of mixed hydroxo complexes (ZnH_{-1}**L3** = Zn**L3**(OH) and ZnH_{-2}**L3** = Zn**L3**$(OH)_2$), similarly to the mononuclear zinc(II) complexes of **L2**.

Interestingly, considerable amount of trinuclear complexes is formed in equimolar solution, according to both potentiometric and NMR data (Figs. 7A and 8C). This indicates that **L3** is able to bind more than one Zn^{2+} with nearly equivalent binding affinities, resulting a significant amount of unbound **L3** above pH 7 in equimolar solution (signals of the free ligand and the fast exchanging monocomplexes manifest as an average). At 3:2 metal-to-ligand ratio, trinuclear complexes become dominant in neutral and basic solutions (Fig. 7B). At pH 6 the parent Zn_3**L3**$_2$ is formed; this stoichiometry implies that the zinc(II) ions are coordinated by two arms of the tripod, originated from either the same or two different ligand molecules (Scheme 4). Such M_3L_2 type cluster formation is well described in the literature regarding tripodal ligand complexes [30], and a similar species was detected in the copper(II)-**L3** system, too [12].

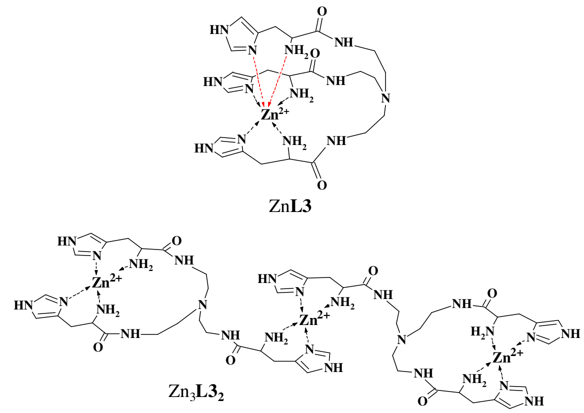

Scheme 4. Proposed structures of mono- and trinuclear Zn(II)-**L3** complexes (one of the two bonds indicated by red dashed arrows may be absent in Zn**L3**).

Since the metal ions in Zn_3**$L3_2$** are coordinated by less nitrogen donors than in Zn**L3**, the trinuclear complex is more prone to deprotonation. The formation of Zn_3H_{-2}**L3**$_2$ and Zn_3H_{-3}**L3**$_2$ results in considerably broadened ^{1}H NMR spectra (Fig. 9). On the other hand, parallel with the formation of Zn_3H_{-4}**L3**$_2$ (pH 8-10) numerous narrow signals appear on the aromatic region. The great number of peaks cannot be explained by the speciation of complexes, since at least 22 different imidazole signals observed at pH 10, which seem to

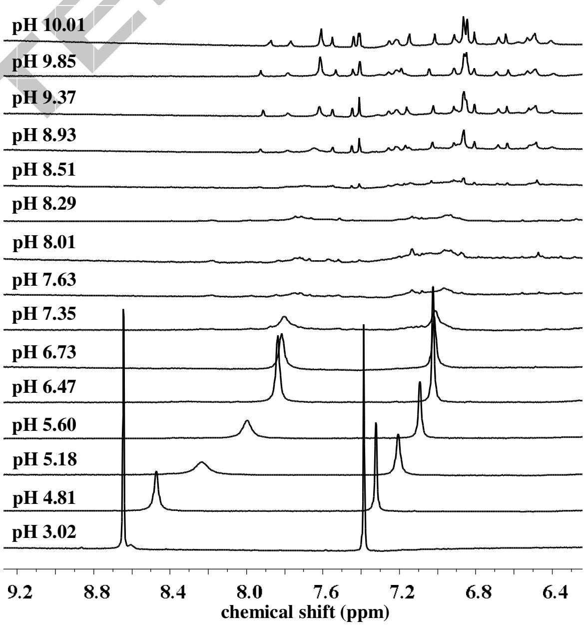

Fig. 9. Aromatic region of the pH dependent ^{1}H NMR spectra of Zn(II)-**L3** 3:2 system (in H_2O/D_2O, $c_{\mathbf{L3}}$ = 0.0023 M, I = 0.1 M NaCl, T = 298 K).

correspond to a single (de)protonation state (at this pH ~95% of zinc(II) is bound in Zn_3H_{-4}**L3**$_2$). Among them, at least 7 different C^2H/C^5H imidazole proton pairs can be identified on the TOCSY spectrum (Fig. S5.3).

The observed multiplication of the signals can imply either the inequivalence of imidazole protons in the trinuclear species due to the conformational differences, or the formation of differently composed $(Zn_3H_{-4}$**L3**$_2)_n$ ($n \geq 1$) oligomer complexes. The size of such oligomers would be high enough to have detectable variance in their hydrodynamic radii. Accordingly, ^1H DOSY measurements were performed, which indicate indeed the presence of several complexes with moderately different diffusion parameters, clearly distinct from that of the free ligand (at 7.61 and 6.85 ppm, Fig. 10).

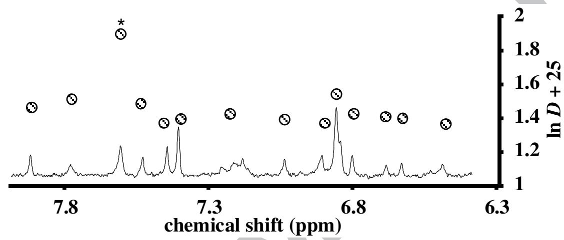

Fig. 10. Aromatic region of ^1H NMR spectra in Zn(II)-**L** 3:2 system, and the measured diffusion coefficients by ^1H DOSY NMR. * indicates the C^2H signal of the free ligand, the corresponding C^5H signal at 6.85 ppm is not resolved (pH = 10, $c_L = 0.0019$ M, $c_{Zn(II)} = 0.0027$ M, $I = 0.1$ M NaCl, $T = 298$ K).

This observation supports the presence of several oligomers with different compositions. Applying the approximate rule $(D_{ref}/D_x)^3 = M_x/M_{ref}$ (where D, M and ref stand for diffusion coefficient, molar mass and reference compound, for which dioxane and acetonitrile were used), one can estimate several oligomers formed by the association of 2-8 trinuclear complexes (although uncertainties must be taken into account due to the non-spherical geometry and different hydration of the ligand and its zinc(II) complexes).

The TOCSY spectrum (Fig. S5.3) indicates that the imidazole C^2H/C^5H signals are scattered in a wide range, similarly to the case of Zn(II)-**L2** 2:1 system. Although the presence of several oligomers and the complexity of the NMR spectra do not allow doubtless identification of the coordinating groups and complex compositions, the broadened signals around pH 8 may indicate mixed hydroxo complexes and even their oligomerization through hydroxo-bridges. However, it seems clear that the formation of Zn_3H_{-4}**L3**$_2$ involves a new type of bridging unit, which results in slow ligand exchange processes. This is in striking resemblance to the Zn(II)-**L2** 2:1 system at basic pH (see Fig. 5 and Electronic Supplementary Information, Section 4.), which might support that imidazolato-bridges participate in the assembly of $(Zn_3H_{-4}\mathbf{L3}_2)_n$ complexes.

Conclusion – *Comparison of zinc(II) binding properties*

The studied three ligands provide a variety of donor sites and consequently, different stability and structure for their zinc(II) complexes, depending on pH and metal-to-ligand ratios. Around pH 5-7, histamine-like coordination is operating in all cases, and the zinc(II) sequestering ability depends on the number of histidyl-functionalized arms (Fig. 11A). Due to the formation of a macrochelate ring between the two $\{N_{im},NH_2\}$ binding sites, the metal ion is bound considerably stronger in ZnH**L2** than in $Zn(histamine)_2$ or $Zn(His\text{-}Gly)_2$. The third histidyl-functionalized arm provides even higher zinc(II) binding ability for **L3**. These observations clearly emphasize the benefits of increasing donor group 'density' of tripodal peptidomimetics.

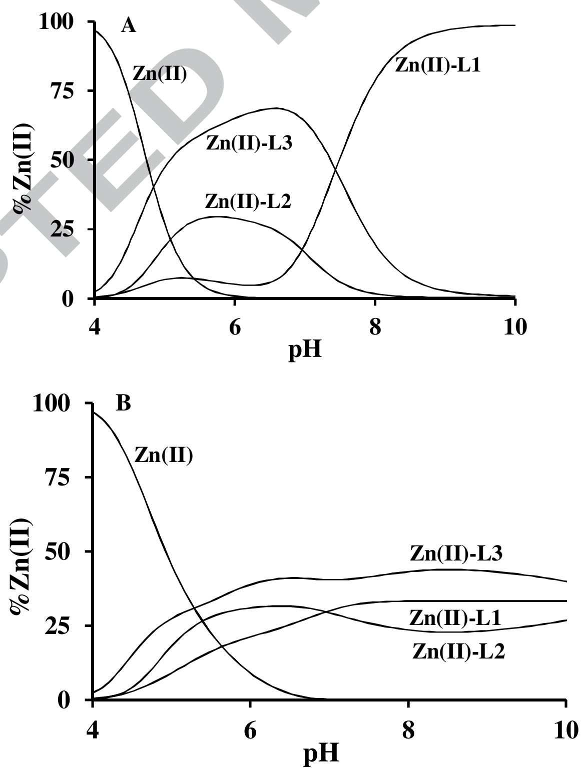

Fig. 11. Predominance diagrams in the Zn(II)-**L1**-**L2**-**L3** quaternary systems at 1:1:1:1 (A) and 3:1:1:1 (B) ratios (c_L = 0.002 M).

The zinc(II) binding properties are fundamentally different at higher pH. The tren-like subunit in **L1** acts as an anchoring site for amide deprotonation. The forming {$3NH_2$,N^-,N_{tert}} type coordination in ZnH_{-1}**L1** results much higher stability as compared with the {NH_2,N^-,N_{im}} bound ZnH_{-1}(Gly-His) species, a rare example where zinc(II)-amide N^- coordination takes place.

Although **L1** provides tight binding above pH 7, it forms only mononuclear species; while the higher levels of functionalization in **L2** and **L3** allow the formation of oligonuclear complexes. At threefold metal excess the three ligands share nearly the same amount of zinc(II) (Fig. 11B). On the other hand, the high histidine 'density' in **L2** and **L3** also provides the formation of imidazolato-bridged oligomerization of di- and trinuclear complexes, which has never been observed before in zinc(II) complexes of simple linear peptides.

Acknowledgements

The research was supported by National Research, Development and Innovation Office-NKFIH through projects GINOP-2.3.2-15-2016-00038, OTKA 101541 and TÉT_15-1-2016-0031. The authors are grateful to S. Poinsignon for her assistance in NMR measurements, F. Lachaud for ESI-MS measurements and S. Parant for technical help at Université de Lorraine.

Appendix A. Supplementary material

Detailed supplementary data associated with this article, including mass and 2D NMR spectra as well as ^{1}H NMR titrations, can be found, in the online version, at ????.

References

[1] Y. Tor, J. Libman, A. Shanzer, C.E. Felder, S. Lifson, J. Am. Chem. Soc. 114 (1992) 6653.

[2] H.B. Albada, R.M.J. Liskamp, J. Comb. Chem. 10 (2008) 814.

[3] J. Kwak, A.D. Capua, E. Locardi, M. Goodman, J. Am. Chem. Soc. 124 (2002) 14085.

[4] C.V. Bonduelle, E.R. Gillies, Pharmaceuticals 3 (2010) 636.

[5] J.R. Hiscock, M.R. Sambrook, P.B. Cranwell, P. Watts, J.C. Vincent, D.J. Xuereb, N.J. Wells, R. Raja, P.A. Gale, Chem. Comm. 50 (2014) 6217.

[6] S. Blanc, P. Yakirevitch, E. Leize, M. Meyer, J. Libman, A. Van Dorsselaer, A.-M. Albrecht-Gary, A. Shanzer, J. Am. Chem. Soc. 119 (1997) 4934.

[7] A. Mohamadou, C. Gerard, J. Chem. Soc., Dalton Trans. (2001) 3320.

[8] A.-S. Jullien, C. Gateau, I. Kieffer, D. Testemale, P. Delangle, Inorg. Chem. 52 (2013) 9954.

[9] H.B. Albada, F. Soulimani, B.M. Weckhuysen, R.M.J. Liskamp, Chem. Comm. (2007) 4895.

[10] M. Gelinsky, R. Vogler, H. Vahrenkamp, Inorg. Chem. 41 (2002) 2560.

[11] M.M. Ibrahim, G.A.M. Mersal, J. Inorg. Biochem. 104 (2010) 1195.

[12] Á. Dancs, N.V. May, K. Selmeczi, Z. Darula, A. Szorcsik, F. Matyuska, T. Páli, T. Gajda, New J. Chem. 41 (2017) 808.

[13] I. Sóvágó, K. Ősz, Dalton Trans. (2006) 3841.

[14] I. Sóvágó, Cs. Kállay, K. Várnagy, Coord. Chem. Rev. 256 (2012) 2225.

[15] D.M. Shendage, R. Fröhlich, G. Haufe, Org. Lett. 6 (2004) 3675.

[16] K.M. DiVittorio, F.T. Hofmann, J.R. Johnson, L. Abu-Esba, B.D. Smith, Bioorg. Med. Chem. 17 (2009) 141.

[17] E. Boseggia, M. Gatos, L. Lucatello, F. Mancin, S. Moro, M. Palumbo, C. Sissi, P. Tecilla, U. Tonellato, G. Zagotto, J. Am. Chem. Soc. 126 (2004) 4543.

[18] F.J.C. Rosotti, H. Rosotti, The determination of stability constants, McGraw-Hill Book Co., New York, 1962.

[19] E. Högfeldt, Stability Constants of Metal-Ion Complexes, Part A. Inorganic Ligands, Pergamon, New York, 1982.

[20] L. Zékány, I. Nagypál, G. Peintler, PSEQUAD for chemical equilibria, Technical Software Distributors, Baltimore, MD, 1991.

[21] R. Mills, J. Phys. Chem. 77 (1973) 685.

[22] A.G. Blackman, Polyhedron 24 (2005) 1.

[23] I. Török, T. Gajda, B. Gyurcsik, G. K. Tóth, A. Péter, J. Chem. Soc. Dalton Trans. (1998) 1205.

[24] D.L. Rabenstein, S.A. Daignault, A.A. Isab, A.P. Arnold, M.M. Shoukry, J. Am. Chem. Soc. 107 (1985) 6435.

[25] T. Gajda, B. Henry, J.-J. Delpuech, Inorg. Chem. 34 (1995) 2455.

[26] K. Selmeczi, P. Gizzi, D. Champmartin, P. Rubini, E. Aubert, S. Dahaoui, B. Henry, Inorg. Chem. 49 (2010) 8222.

[27] E. Farkas, I. Sóvágó, A. Gergely, J. Chem. Soc., Dalton Trans. (1983) 1545.

[28] A. Myari, G. Malandrinos, Y. Deligiannakis, J.C. Plakatouras, N. Hadjiliadis, Z. Nagy, I. Sóvágó, J. Inorg. Biochem. 85 (2001) 253.

[29] D. Árus, A. Jancsó, D. Szunyogh, F. Matyuska, N.V. Nagy, E. Hoffmann, T. Körtvélyesi, T. Gajda, J. Inorg. Biochem. 106 (2012) 10.

[30] Q.H. Chen, L. Chen, F.L. Jiang, M.C. Hong, Chem. Rec. 15 (2015) 711.

In order to establish how the increasing donor group 'density', *i.e.* the gradual N-histidyl substitution, alters the coordination chemical properties of the tripodal platform, we synthesized mono-, bis- and tris(L-histidyl)-functionalized tren derivatives, and studied their zinc(II) complexes. The three ligands provide a variety of donor sites, and consequently different stability and structure for their zinc(II) complexes depending on the pH and metal-to-ligand ratios.

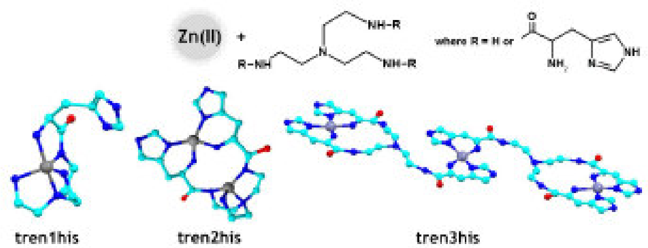

Highlights

- The studied ligands provide a variety of donor sites, hence stability and structure for zinc(II)
- Around pH 5-7, histamine-like coordination is operating in all cases
- The *mono*-(L-histidyl)-functionalized tren (**L1**) forms a unique {$3NH_2$,N^-,N_{tert}} type coordination
- The high histidine 'density' in **L2** and **L3** results in imidazolato-bridged oligomers